Understanding chemical enhancements of surface-enhanced Raman scattering using a Raman bond model for extended systems

Ran Chen¹ and Lasse Jensen^{1, a)}

Department of Chemistry, Pennsylvania State University, University Park,

Pennsylvania 16802, United States

(Dated: 16 December 2024)

In this work, we extend a previously developed Raman bond model to periodic slab systems for interpreting chemical enhancements of surface-enhanced Raman scattering (SERS). The Raman bond model interprets chemical enhancements as interatomic charge flow modulations termed Raman bonds. Here, we show that the Raman bond model offers a unified interpretation of chemical enhancements for localized and periodic systems. As a demonstration of the Raman bond model, we study model systems consisting of CO and pyridine molecules on Ag clusters and slabs. We find that for both localized and periodic systems the dominant Raman bonds are distributed near the molecule-metal interface and therefore the chemical enhancements are determined by a common Raman bond pattern. The effects of surface coverages, thickness, and roughness on the chemical enhancements are studied, which shows that decreasing surface coverages or creating surface roughness increases chemical enhancements. In both of these cases, the inter-fragment charge flow connectivity is improved due to more dynamic polarization at the interface. The chemical enhancement is shown to scale with the inter-fragment charge flow to the fourth power. Since the inter-fragment charge flow is determined by the charge transfer excitation energy, the Raman bond model is connected to the transition based analysis of chemical enhancements. We also show that the SERS spectra of localized and periodic systems normalized by inter-fragment charge flows can be unified. In summary, the Raman bond model offers a unique framework for understanding SERS spectra in terms of Raman bond distributions and offers a connection between localized and periodic model systems of SERS studies.

a) Electronic mail: jensen@chem.psu.edu

I. INTRODUCTION

Surface-enhanced Raman scattering (SERS) is widely applied because of its high sensitivity and chemical specificity. 1–12 SERS enhancements arise from two complementary mechanisms, electromagnetic mechanism (EM) and chemical mechanism (CM). In EM, SERS enhancements are explained by local electric field enhancements due to surface plasmons. As SERS enhancements approximately scale with field enhancements to the fourth power, EM can be applied to explain the high sensitivity of SERS. 9,11–15 However, SERS spectral signatures cannot be explained fully by only invoking EM because chemical interactions between molecules and metal are usually neglected in EM. The chemical specificity of SERS enhancements is mainly explained by CM, where SERS enhancements are attributed to bonding interactions between molecules and metal. 15–18

Because of the chemical specificity, first principles simulations are essential for understanding CM.^{19–29} To model SERS spectra using first principles simulations, localized clusters^{19–25} or periodic slabs^{26–29} are applied. Clusters are applied because they offer local approximations of surface defects or protrusions and provide multiple kinds of binding sites. The finite size effect of cluster models can be avoided by adopting slab models due to periodic boundary conditions. The frequency dependence and selection rules of SERS spectra can be explained by the sumover-states formula of Raman scattering.^{30–36} In particular, it offers a unified description of SERS enhancements and shows the charge transfer contributions to chemical enhancements. However, including all states in the formula is computationally intractable for SERS systems and thus only a few states are typically included. For example, the sum-over-states formula can be simplified to a two state model, which estimates the average chemical enhancements by energy alignment of molecular frontier orbitals with respect to the Fermi level.^{20–22} However, the two state model cannot explain SERS spectral signatures because it does not provide a quantitative explanation of the mode specific enhancements.

To get an intuitive and quantitative interpretation of chemical enhancements, we have developed a Raman bond model for localized systems.^{37,38} The analysis of electronic transitions in the sum-over-states formula is avoided in the Raman bond model and instead polarizability derivatives are expressed as interatomic charge flow modulations by distributing induced atomic charges with a penalty on long range charge flows. We have demonstrated that the off resonance enhancements can be explained by the Raman bonds distributed near the molecule-metal interface.³⁷ The model

was further applied to explain the frequency dependence of SERS enhancements by connecting Raman bond distributions with different resonance contributions.³⁸ Besides localized systems, periodic systems have also been applied to study SERS as macroscopic SERS systems can be modeled by small systems with dozens of atoms in the unit cells with periodic boundary condition, and the edge effect of finite clusters can be avoided by using periodic slabs. Thus, in this work, we extend the Raman bond model to periodic systems so that we achieve a unified interpretation of chemical enhancements for both localized and periodic systems. To demonstrate the unified interpretation provided by the Raman bond model, model systems with CO and pyridine molecules on Ag clusters and slabs are studied. We will study the effects of surface coverage, thickness, and roughness on chemical enhancements using slab models and compare the results with cluster models.

II. THEORY

The Raman bond model partitions the polarizability derivative into atomic and bond contributions, termed Raman atoms and bonds:

$$\frac{\partial \alpha_{ab}}{\partial Q_k} = \sum_{i} \frac{\partial \{-\int (\mathbf{r}_b - \mathbf{R}_{i,b}) \delta \rho_{i,a} d\mathbf{r}\}}{\partial Q_k} + \sum_{ij,j>i} \frac{\partial \{q_{ij,a} (\mathbf{R}_{i,b} - \mathbf{R}_{j,b})\}}{\partial Q_k}, \tag{1}$$

where a, b are directions in Cartesian space. α_{ab} is one component of a polarizability tensor and Q_k is a vibrational mode. r and R are electronic and nuclear coordinates, respectively. $\delta \rho_{i,a}$ is the electron density of atom i induced in the direction a. $q_{ij,a}$ is the charge flow in direction a between atom i and j. Raman atoms correspond to modulations of induced atomic dipoles and Raman bonds correspond to modulations of interatomic charge flows. Raman atoms and bonds can be mapped onto the system structure and visualized as spheres and cylinders, whose volumes represent magnitudes of the contributions and colors represent phases of the contributions. In this work, atomic charges are calculated using the Hirshfeld charge model³⁹ and charge flows are calculated using the Loprop method⁴⁰ where a penalty function is applied to minimize long range charge flows:

$$f(R_{ij}) = \begin{cases} \exp\{c_1 \times (\frac{R_{ij}}{R_i^{\text{cov}} + R_j^{\text{cov}}})^2\} & \text{if } R_{ij} < 1.1(R_i^{\text{cov}} + R_j^{\text{cov}}) \\ \exp\{2c_1 \times (\frac{R_{ij}}{R_i^{\text{cov}} + R_j^{\text{cov}}})^2\} & \text{if } R_{ij} \ge 1.1(R_i^{\text{cov}} + R_j^{\text{cov}}) \end{cases},$$
(2)

where R_{ij} is the distance between atom i and j, R_i^{cov} is covalent radius of atom i,⁴¹ and c_1 is a coefficient that controls the penalty on long range charge flows.

For bonds perpendicular to the polarization direction we have $R_{i,b} - R_{j,b} = 0$ and therefore $q_{ij,a}(R_{i,b} - R_{j,b})$ would be zero and not contribute to the polarizability. Therefore charge flows perpendicular to the polarization direction need to be minimized, which can be done by including extra penalty on charge flows perpendicular to the polarization direction. For a localized system, bonds perpendicular to the polarization direction are few and no extra penalty is needed to reproduce the total polarizability. However, for a periodic slab system polarized in the out of plane direction, a significant number of bonds are perpendicular to the polarization direction and the extra penalty is needed for the periodic system to reproduce the total polarizability. Accordingly, the penalty function is modified as:

$$f(R_{ij}, \theta_{ij}) = \begin{cases} \exp\{c_1 \times (\frac{R_{ij}}{R_i^{\text{cov}} + R_j^{\text{cov}}})^2\} + \exp\{c_2(1 - \cos\theta_{ij})\} & \text{if } R_{ij} < 1.1(R_i^{\text{cov}} + R_j^{\text{cov}}) \\ \exp\{2c_1 \times (\frac{R_{ij}}{R_i^{\text{cov}} + R_j^{\text{cov}}})^2\} + \exp\{c_2(1 - \cos\theta_{ij})\} & \text{if } R_{ij} \ge 1.1(R_i^{\text{cov}} + R_j^{\text{cov}}) \end{cases},$$
(3)

where θ_{ij} is the angle between the bond connecting atom i and j and the polarization direction. c_2 is a coefficient that controls the penalty on charge flows perpendicular to the polarization direction. A test of penalty coefficients is given in the supporting information and based on the test results we adopt $c_1 = 1$ and $c_2 = 3$ for all systems in this work.

When charge flows are calculated for a periodic slab system, a (3×3) super cell is constructed, to which the Loprop method with the modified penalty function is applied. Further increasing the super cell size does not significantly change charge flows. To avoid double counting, charge flows between the central cell and half of the neighboring cells are accounted and a full charge flow network is achieved by translations along slab lattices.

III. COMPUTATIONAL DETAILS

Calculations in this work were performed using a local version of BAND program package 42,43 for the periodic systems and a local version of the Amsterdam density functional (ADF) program package for the localized systems. 44,45 The Becke-Perdew (BP86) XC-potential 46,47 and triple- ζ polarized slater type (TZP) basis set with large frozen cores from the ADF basis set library were used. The scalar relativistic effects were accounted for by the zeroth-order regular approximation (ZORA) 48 . Full geometry optimization were performed for Ag slabs and Ag clusters. To avoid surface reconstruction, adatoms were relaxed with the underlying slabs fixed. For any system in this work, the molecule-metal axis was aligned with the z axis and only the zz components of the

polarizabilities were considered as this choice is consistent with the SERS surface selection rule. To eliminate the geometric effect when comparing the slabs and clusters, the same molecular configuration and normal mode displacements were chosen. For the CO-Ag systems, the CO was put on the atop site and aligned in the z direction with C-Ag bond length of 2.2967 Åand C-O bond length of 1.1474 Å. The Ag-C and C-O bond lengths were tested on different Ag surfaces. On all the Ag surfaces, the C-O bond length variation where on the order of 10^{-4} Ångstrom. On the Ag surfaces with no adatom, the Ag-C bond length had variation on the order of 10^{-3} Ångstrom. These small changes of bond lengths led to insignificant effect on the Raman intensities. When the adatom was introduced, the Ag-C bond length decreased about 0.2 angstrom, which decreased the Raman intensity. However, applying the same bond length to the CO-Ag systems with adatoms did not change any conclusions in this work. Geometry optimization and normal mode analysis was conducted for pyridine on the Ag slab, and the same geometry and normal modes were applied to the pyridine on the Ag cluster. The geometry of the pyridine optimized on the slab is quite similar to the geometry of the pyridine optimized on the cluster. The root-mean-square deviation of atomic positions for the pyridine optimized on the slab versus the pyridine optimized on the cluster was about 0.05 Ångstrom. For the cluster system, adopting the geometry and normal modes of the pyridine on the slab barely changed the vibrational frequencies or the spectral signatures, while slightly decreased the Raman intensities. Applying the same surface configurations and normal modes for the CO-Ag systems or the pyridine-Ag systems serves the purpose of eliminating the geometric effect on enhancements and emphasizing on how enhancements are influenced by different surface models. The energy of incident light in this work was 0 eV, and applied to all systems. The Ag excited states were not on resonance, and enhancements were studied at the static limit, which are usually considered to be chemical enhancements. Polarizabilities were calculated by the finite differentiation of dipoles versus electric fields with a step size of 0.001 atomic unit. Polarizability derivatives were calculated by the finite differentiation of polarizabilities with respect to normal mode displacements. All Raman bond figures in this work were plotted using PyMOL⁴⁹.

IV. RESULTS AND DISCUSSION

To demonstrate how the Raman bond model can be used to interpret chemical enhancements of periodic systems, systems with CO on different Ag slabs are studied. We start with a (2×2)

2-layer Ag(111) slab (Fig.1 (a)), which provides an enhancement factor (EF) of 4. The Raman bond pattern of CO on the (2×2) 2-layer slab (Fig.1 (a)) shows that the chemical enhancement is determined by the Raman bonds distributed near the molecule-metal interface. The pattern can be explained as the molecular vibration mainly modulate the charge flows near the molecule-metal interface and the extra charge flow modulations compared with the free molecule leads to the chemical enhancement. Next, to study the effect of slab thickness on the chemical enhancement, we add two layers of Ag atoms to the slab and construct a (2×2) 4-layer Ag(111) slab (Fig.1) (b)). The thicker slab provides an EF of 3, which means that increasing the slab thickness has a trivial effect on the chemical enhancement. The effect of slab thickness is explained by the change of the Raman bond pattern. The Raman bond pattern in Fig.1 (b) shows that adding two layers of Ag atoms barely changes the Raman bond pattern and Raman bonds in the new added Ag layers are destructive and have negligible magnitudes. The Raman bond analysis can be simplified to analyzing the enhancement contributions from the molecule, the inter-fragment bond, and the metal by grouping Raman atoms and bonds in the corresponding parts of the system. Adding two layers of Ag atoms does not change the molecular contribution, and decreases the contributions of the inter-fragment bond and the metal by 6% and 8% respectively. The change of the three contributions shows that increasing the slab thickness barely affects the charge flow modulations near the interface. Such minor change can be attributed to the slight change of the inter-fragment charge flow as adding two layers of Ag atoms increases the inter-fragment charge flow only by 5%. The almost unchanged inter-fragment charge flow connectivity does not help the molecular vibration to modulate more charge flows near the interface. The effect of slab thickness can be further explained as the charge flows in the bottom layers of the slab cannot respond effectively or coherently to the vibrational modulation due to the screening of the charge flows in the top layers. Next, to study the effect of surface roughness, we add an adatom to the slab and construct a $(2 \times$ 2) 2-layer Ag(111) slab with an adatom (Fig.1 (c).). The slab with an adatom provides an EF of 13, which means that creating surface roughness effectively increases the chemical enhancement. The Raman bond pattern in Fig.1 (c) helps explain the chemical enhancement change by showing that the adatom leads to new constructive Raman bonds between the adatom and the Ag atoms underneath and destructive Raman bonds in the metal become weaker. Introducing an adatom increases the contributions of the molecule, the inter-fragment bond, and the metal by 17%, 20%, and 99% respectively. The effect of surface roughness can also be explained by the change of interfragment charge flow. Introducing an adatom increases the inter-fragment charge flow by 48%.

The increased inter-fragment charge flow due to the surface roughness leads to more effective and coherent charge flow modulations across the interface, which increases the chemical enhancement.

The Raman bond model also bridges CM studies using localized clusters and periodic slabs. CO on a surface and a vertex of a tetrahedral Ag₂₀ cluster are studied, whose structures are shown in Fig.1 (d) and (e) respectively. The surface binding site provides an EF of 38 and the vertex binding site provides an EF of 1885. The chemical enhancement difference is explained by the Raman bond patterns in Fig.1 (d) and (e), where the vertex binding site leads to more and stronger constructive Raman bonds than the surface binding site. The explanation of the surface roughness effect on chemical enhancements for the periodic systems is also valid for the localized systems. Namely, the vertex binding site reflects increased surface roughness and leads to a larger inter-fragment charge flow than the surface binding site. The better inter-fragment charge flow connectivity better connects charge flows across the interface. Consequently, more effective and coherent charge flows are created and a larger chemical enhancement is achieved. The simulation results indicate that to increase the chemical enhancement, it is more effective to create surface roughness than increasing slab thickness. This finding is consistent with the previous literature 50,51 that adatoms provide active sites of SERS enhancements. According to EM, we know that surface roughness creates hot spots of EM enhancements where local fields are significantly enhanced. 13 In this work, we show that surface roughness also creates hot spots of chemical enhancements where the inter-fragment charge flow connectivity is significantly improved. It should be noted that improving the inter-fragment charge flow connectivity does not necessarily increase overall SERS enhancements because EM enhancements can decrease when the inter-fragment charge flow connectivity is improved³⁸. Despite that chemical enhancements of the systems in Fig. 1 (a) - (e) range over three orders of magnitude, a common Raman bond pattern is found for both localized and periodic systems. The chemical enhancement of a SERS system is determined by the Raman bonds distributed near the molecule-metal interface. A cone-shaped network of constructive Raman bonds is formed in the metal. Improving the inter-fragment charge flow connectivity enhances Raman bonds and expands constructive Raman bonds in the metal, which leads to a larger chemical enhancement.

Next, CO on a (4×4) 2-layer Ag slab with an adatom is studied (1 (f)) and this slab provides an EF of 261. If we consider that the larger unit cell models a lower surface coverage, the simulation result indicates that a low surface coverage combined with surface roughness further increases the chemical enhancement. The extra increase of the chemical enhancement can be ex-

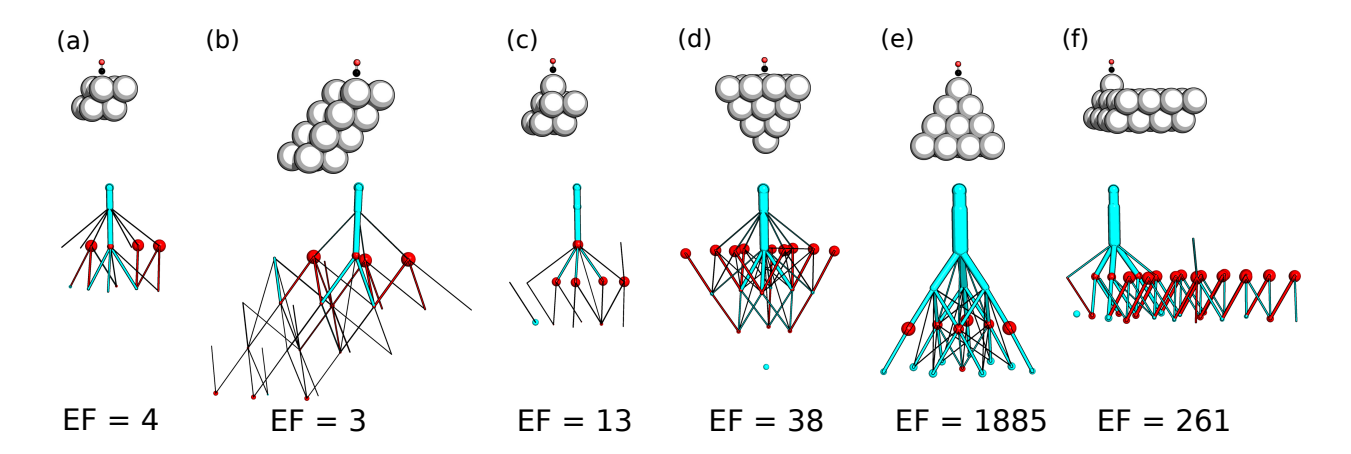


FIG. 1. Structure diagrams and Raman bond patterns of CO on a (2×2) 2-layer slab, a (2×2) 4-layer slab, a (2×2) 2-layer slab with an adatom, a surface of Ag₂₀, a vertex of Ag₂₀, and a (4×4) 2-layer slab with an adatom are shown in (a), (b), (c), (d), (e), (f) respectively. Raman atoms and bonds are visualized as spheres and cylinders, whose volumes represent magnitudes of the contributions and colors represent phases of the contributions. In this work, the constructive and destructive Raman bonds are colored blue and red respectively.

plained by the Raman bond pattern shown in Fig.1 (f). Compared with CO on the (2×2) 2-layer Ag slab, the lower surface coverage with surface roughness leads to enhanced Raman bonds across the system and more constructive Raman bonds in the metal. The contributions of the molecule, the inter-fragment bond, and the metal are increased by 2 times, 5 times, and 4 times respectively. Such Raman bond pattern can also be explained by the improved inter-fragment charge flow connectivity. Compared with CO on the (2×2) 2-layer Ag slab, this slab almost doubles the inter-fragment charge flow. The improved inter-fragment charge flow connectivity leads to more effective and coherent charge flow modulations and consequently a larger chemical enhancement. Another interesting observation is that for the periodic system at a low surface coverage, a ripple like pattern of Raman bonds centering the molecule-metal interface is observed, in which Raman bond magnitudes decay from the interface and Raman bond phases fluctuate.

To study the effect of surface coverages on chemical enhancements in detail, we construct CO on 2-layer Ag(111) slabs with different unit cell sizes. Polarizability derivatives of the CO-Ag systems are plotted versus the unit cell sizes in Fig. 2 (a). The simulation results show that the chemical enhancement per molecule increases and saturates when the surface coverage decreases. The highest coverage where CO occupies each atop site of the Ag slab predicts an EF smaller than 1. To understand this, we compare the Raman bond patterns of the CO-Ag systems, which can be

simplified by analyzing the contributions of the molecule, the inter-fragment bond, and the metal of the CO-Ag systems. The contributions are plotted versus the unit cell sizes in Fig. 2 (b). Fig. 2 (b) shows that the contributions of the molecule and the inter-fragment bond are constructive and the metal contribution is destructive. As the surface coverage decreases, the contributions from the molecule and the inter-fragment bond increase while the contribution from the metal decreases. Such pattern can be explained by the changes of the inter-fragment charge flows at different surface coverages. When the surface coverage is decreased, the inter-fragment charge flow is increased for each CO molecule, which leads to more effective charge flow modulations across the interface and thus a larger enhancement per molecule. In contrary, when the surface coverage is increased, the inter-fragment charge flow is decreased for each CO molecule, which limits charge flow modulations across the interface and leads to a smaller enhancement per molecule. At the highest coverage case, the inter-fragment charge flow connectivity is the poorest as on average each CO only perturbs charge flows in two Ag atoms. As a consequence, the charge flow modulations across the interface are most limited and an EF smaller than 1 is achieved. Fig. 2 (b) shows that the flat slabs have destructive metal contributions and decreasing the surface coverage decreases the metal contribution. However, the metal contributions of the slabs with adatoms (Fig.1 (c) and (f)) are constructive and decreasing the surface coverage increases the metal contribution. Although, the overall intensity increases with lowering the surface coverage for both kinds of slabs, the increase is larger for the slabs with adatoms due to their constructive metal contributions. Despite that it is difficult to correlate enhancements with surface coverages experimentally, our finding indicates that to achieve large chemical enhancements per molecule, it is advantageous to adopt low surface coverages. It is worth noting that in the simulations, the CO molecules on the slab vibrate synchronously because of the periodic boundary condition, and in reality the CO molecules on the surface can vibrate asynchronously. As vibrations of CO molecules can be asynchronous, for the high coverage cases, the interfacial charge flows may be better described via larger unit cells with many CO molecules than the very small unit cells.

In the above discussions, we have shown that better charge flow connectivity leads to larger chemical enhancements for both localized and periodic systems. To get a more quantitative correlation between chemical enhancements and inter-fragment charge flows, we study polarizability derivatives and inter-fragment charge flows of CO on different Ag slabs and clusters. The polarizability derivatives of CO on different Ag slabs and clusters are plotted versus their squared inter-fragment charge flows in Fig. 3 (a). We observe a linear trend between the polarizability

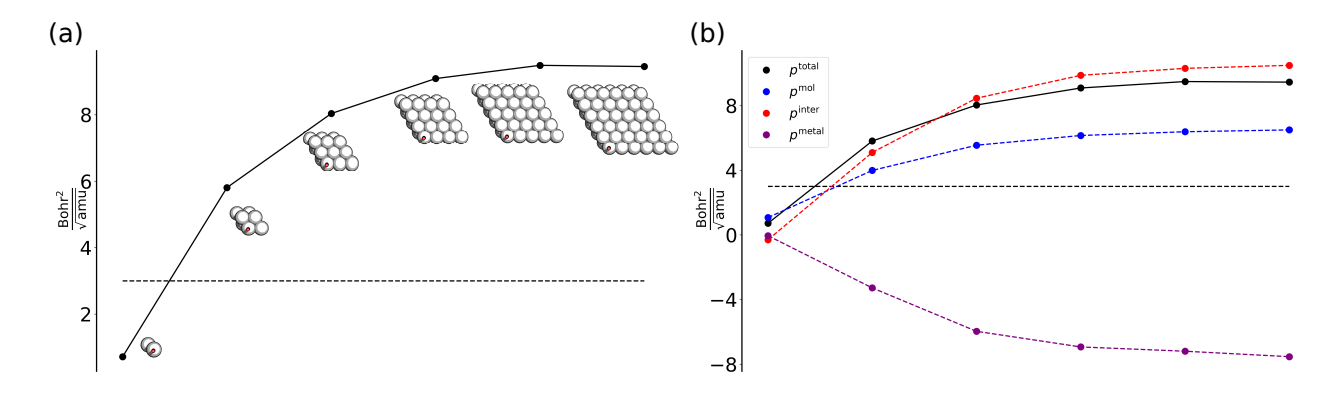


FIG. 2. Polarizability derivatives of CO on Ag(111) slabs are plotted versus unit cell sizes in (a). Top views of the structures of the CO-Ag systems are shown next to corresponding data points. Total polarizability derivatives (p^{total}) and contributions from the molecule (p^{mol}), the inter-fragment bond (p^{inter}), and the metal (p^{metal}) of the CO-Ag systems are plotted versus unit cell sizes in (b). The horizontal dashed lines in (a) and (b) show the polarizability derivative of a free CO.

derivatives and the squared inter-fragment charge flows of the CO-Ag systems. To explain the quadratic relation, we refer to a two state model of chemical enhancements.²⁰ The previous work shows that approximately, the polarizability derivative of a SERS system is inversely proportional to the squared charge transfer excitation energy. Since decreasing the charge transfer excitation energy increases the inter-fragment charge flow, it follows that the inter-fragment charge flow is inversely proportional to the charge transfer excitation energy. Thus, we would have that the polarizability derivative is proportional to the squared inter-fragment charge flow. Therefore, the Raman bond model and the two state model predict a similar trend. Because the Raman intensity is proportional to the squared polarizability derivative, the chemical enhancement would be proportional to the inter-fragment charge flow to the fourth power. Larger chemical enhancements can be achieved by improving the inter-fragment charge flow connectivity.

To explain the quadratic relation between the polarizability derivatives and the inter-fragment charge flows of the CO-Ag systems, we plot the contributions of the molecule, the inter-fragment bond, and the metal versus the squared inter-fragment charge flows in Fig. 3 (b), (c), (d) respectively. The figures show that the metal contribution is dominant and determines the quadratic relation between the polarizability derivatives and the inter-fragment charge flows, especially when the inter-fragment charge flow connectivity is good. The metal contribution is dominant because the metal provides a large reservoir of charge flows and the good connectivity allows effective and coherent modulations on these charge flows by the molecular vibration. The contributions of the

molecule and the inter-fragment bond show a better linear trend versus the inter-fragment charge flow, which is shown in the supporting information. When the inter-fragment charge flow connectivity is poor, the contributions of the molecule and the inter-fragment bond become significant. The metal contribution is limited because the poor connectivity does not allow the molecular vibration to effectively modulate the charge flows in the metal. Improving the inter-fragment charge flow connectivity at this case also mainly increases the contributions of the molecule and the inter-fragment bond. The increase of the metal contribution is inhibited because of the interference between the destructive and constructive Raman bonds in the metal. The scaling of the metal contribution implies that adopting small metal clusters in CM studies may lead to underestimated chemical enhancements as limited charge flows are provided by the metal. However, the GGA functionals in DFT simulations can overestimate inter-fragment charge flows and thus chemical enhancements. The deficiency of GGA functionals may compensate the limit of small clusters for estimating chemical enhancements.

The enhancements studied at the static limit are usually considered to be chemical enhancements which is consistent with the definition using in the two-state model. In previous work, we used a frequency-dependent Raman bond³⁸, to establish definition of chemical and electromagnetic enhancements based on the spatial distributions of Raman bonds. Namely, the Raman bonds in the molecule, the inter-fragment bond, and the metal correspond to enhancement contributions of the molecular resonance, the charge transfer resonance, and the surface plasmon resonance. However, only in the limit of no charge-transfer between the two systems can the EM enhancements calculated by the Raman bonds be directly compared with the EM definition arising from classic electrodynamics. In the static limit the Raman bonds in the metal originate from the charge-flow between the two systems which is also reflected in the decay of the Raman bonds in the metal away from the molecule. In contrast, on resonance with the metal excitation the Raman bonds are distributed throughout the metal cluster consistent an EM enhancement. Thus in this work, the Raman bonds, even the Raman bonds in the metal, are considered to contribute to chemical enhancements as the metal resonances are not excited.

To demonstrate that the correlation between chemical enhancements and inter-fragment charge flows is not only unique to the CO-Ag systems, we study pyridine molecules on a (3×3) 2-layer Ag(111) slab and a surface of the Ag₂₀ cluster. The structures of the systems are shown in Fig. 4 (a) and (b) respectively. The polarizability derivatives of the systems are plotted versus the vibrational frequencies in Fig. 4 (c). Fig. 4 (c) shows that the localized system has larger chemical

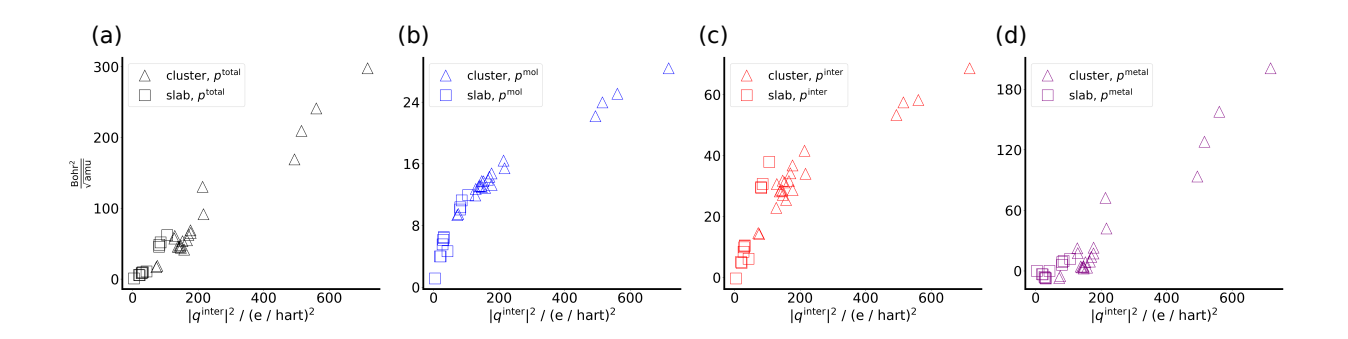


FIG. 3. Polarizability derivatives (p^{total}) are plotted versus squared inter-fragment charge flows ($|q^{\text{inter}}|^2$) for CO on different Ag clusters and slabs in (a). Molecule (p^{mol}), inter-fragment bond (p^{inter}), and metal (p^{metal}) contributions are plotted versus squared inter-fragment charge flows ($|q^{\text{inter}}|^2$) for the CO-Ag systems in (b), (c), (d) respectively.

enhancements than the periodic system. Meanwhile the localized and periodic systems have similar spectral line shapes. Considering that the localized system has a larger inter-fragment charge flow, the larger chemical enhancements of the localized system can be attributed to more effective and coherent charge flow modulations across the interface. We then normalize the polarizability derivatives by the squared inter-fragment charge flows and plot the normalized polarizability derivatives versus the vibrational frequencies in Fig.4 (d) and (e). We observe that the spectra of the periodic and localized systems are better matched when the polarizability derivatives are normalized by the squared inter-fragment charge flows. The major Raman active vibrations with ring stretching around 605, 986, 1020, 1060, and 1578 cm⁻¹ are well matched between the periodic and localized systems. For vibrations around 1202 and 1463 cm⁻¹, which mainly involve C-H bending, the periodic system has larger normalized polarizability derivatives than the localized system. Thus the quadratic relation between the polarizability derivatives and the inter-fragment charge flows shown in the CO-Ag systems is also observed in the pyridine-Ag systems. Although chemical enhancements predicted by the periodic and localized systems are different, SERS spectra of localized and periodic systems normalized by the inter-fragment charge flows can be unified.

V. CONCLUSION

In this work, we extend a Raman bond model to periodic systems. Therefore chemical enhancements of both localized and periodic systems can be consistently interpreted as interatomic charge flow modulations termed Raman bonds. We show a common Raman bond pattern for

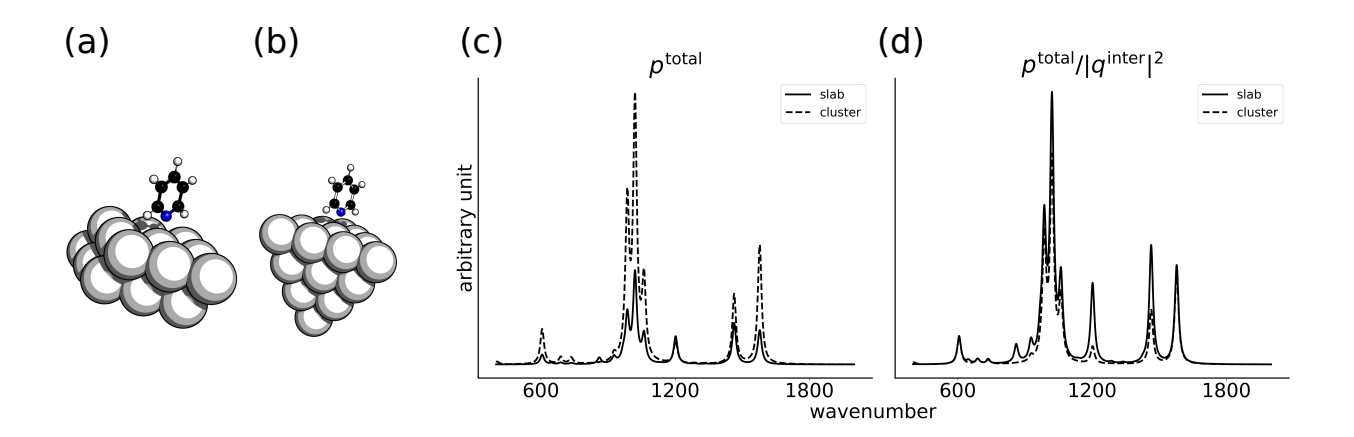


FIG. 4. Structures of pyridine molecules on a (3×3) Ag(111) slab with 2 layers of Ag atoms and a surface of the Ag $_{20}$ cluster are shown in (a) and (b). The polarizability derivatives are plotted versus the vibrational frequencies for the periodic and localized systems in (c). The polarizability derivatives normalized by the squared inter-fragment charge flows are plotted in (d).

both localized and periodic systems that the chemical enhancement is determined by the Raman bonds distributed near the molecule-metal interface. The effects of surface coverages, thickness, and roughness on chemical enhancements are interpreted by Raman bond patterns and explained by changes of inter-fragment charge flow connectivity. Decreasing the surface coverage or creating surface roughness improves the inter-fragment charge flow connectivity and leads to larger chemical enhancements. We also show a linear correlation between chemical enhancements and inter-fragment charge flows to the fourth power. Such correlation is connected to the transition based analysis of chemical enhancements. We also show that SERS spectra of localized and periodic systems can be unified by normalizing the polarizability derivatives with the squared interfragment charge flows. The Raman bond model provides an intuitive and unified interpretation of chemical enhancements for both localized and periodic systems. Such framework is promising to help interpret chemical enhancements of semiconductor substrates, where the effects of binding sites, doping, and defects can potentially be explained by changes of inter-fragment charge flow connectivity.

VI. SUPPLEMENTARY MATERIAL

See the supplementary material for a test of penalty coefficients, a plot of the contributions of the molecule, the inter-fragment bond, and the metal versus the inter-fragment charge flow for the CO-Ag systems, and a top view of the Raman bond pattern of the slab system in Fig.1(f).

ACKNOWLEDGMENTS

The authors gratefully acknowledge financial support from National Science Foundation Grant CHE-2106151. Simulations in this work were conducted in part with Advanced Cyber infrastructure computational resources provided by the Institute for Cyber-Science at The Pennsylvania State University (https://ics.psu.edu/).

REFERENCES

- ¹C. Zong, M. Xu, L.-J. Xu, T. Wei, X. Ma, X.-S. Zheng, R. Hu, and B. Ren, "Surface-enhanced raman spectroscopy for bioanalysis: Reliability and challenges," Chem. Rev. **118**, 4946–4980 (2018).
- ²Z. Wang, S. Zong, L. Wu, D. Zhu, and Y. Cui, "Sers-activated platforms for immunoassay: Probes, encoding methods, and applications," Chem. Rev. **117**, 7910–7963 (2017).
- ³A. M. Shrivastav, U. Cvelbar, and I. Abdulhalim, "A comprehensive review on plasmonic-based biosensors used in viral diagnostics," Commun. Biol. **4**, 70 (2021).
- ⁴B. Sharma, R. R. Frontiera, A.-I. Henry, E. Ringe, and R. P. Van Duyne, "Sers: Materials, applications, and the future," Mater. Today **15**, 16–25 (2012).
- ⁵M. Vendrell, K. K. Maiti, K. Dhaliwal, and Y.-T. Chang, "Surface-enhanced raman scattering in cancer detection and imaging," Trends in Biotechnology **31**, 249–257 (2013).
- ⁶H.-L. Liu, J. Cao, S. Hanif, C. Yuan, J. Pang, R. Levicky, X.-H. Xia, and K. Wang, "Size-controllable gold nanopores with high sers activity," Anal. Chem. **89**, 10407–10413 (2017).
- ⁷S. H. Yazdi and I. M. White, "Optofluidic surface enhanced raman spectroscopy microsystem for sensitive and repeatable on-site detection of chemical contaminants," Anal. Chem. **84**, 7992–7998 (2012).
- ⁸E. C. Le Ru and P. G. Etchegoin, "Single-molecule surface-enhanced raman spectroscopy," Ann. Rev. Phys. Chem. **63**, 65–87 (2012).
- ⁹J. Langer, D. Jimenez de Aberasturi, J. Aizpurua, R. A. Alvarez-Puebla, B. Auguié, J. J. Baumberg, G. C. Bazan, S. E. J. Bell, A. Boisen, A. G. Brolo, J. Choo, D. Cialla-May, V. Deckert, L. Fabris, K. Faulds, F. J. García de Abajo, R. Goodacre, D. Graham, A. J. Haes, C. L. Haynes,

- C. Huck, T. Itoh, M. Käll, J. Kneipp, N. A. Kotov, H. Kuang, E. C. Le Ru, H. K. Lee, J.-F.
- Li, X. Y. Ling, S. A. Maier, T. Mayerhöfer, M. Moskovits, K. Murakoshi, J.-M. Nam, S. Nie,
- Y. Ozaki, I. Pastoriza-Santos, J. Perez-Juste, J. Popp, A. Pucci, S. Reich, B. Ren, G. C. Schatz,
- T. Shegai, S. Schlücker, L.-L. Tay, K. G. Thomas, Z.-Q. Tian, R. P. Van Duyne, T. Vo-Dinh,
- Y. Wang, K. A. Willets, C. Xu, H. Xu, Y. Xu, Y. S. Yamamoto, B. Zhao, and L. M. Liz-Marzán, "Present and future of surface-enhanced raman scattering," ACS Nano **14**, 28–117 (2020).
- ¹⁰L. Wonkyoung, K. Byoung-Hoon, Y. Hyunwoo, P. Moonseong, K. J. Hyun, C. Taerin, J. Yong, K. B. Kyu, and J. Ki-Hun, "Spread spectrum sers allows label-free detection of attomolar neurotransmitters," Nat Commun. 12, 159 (2021).
- ¹¹S. Schlücker, "Surface-enhanced raman spectroscopy: Concepts and chemical applications," Angew. Chem., Int. Edit. **53**, 4756–4795 (2014).
- ¹²W. Xiang, H. Sheng-Chao, H. Shu, Y. Sen, and R. Bin, "Fundamental understanding and applications of plasmon-enhanced raman spectroscopy," Nat. Rev. Phys. **2**, 253–271 (2020).
- ¹³E.-M. Y. e. a. Song Yuan Ding, "Electromagnetic theories of surface-enhanced raman spectroscopy," Chem. Soc. Rev. 46, 4042–4076 (2017).
- ¹⁴J.-M. Nam, J.-W. Oh, H. Lee, and Y. D. Suh, "Plasmonic nanogap-enhanced raman scattering with nanoparticles," Acc. Chem. Res. **49**, 2746–2755 (2016).
- ¹⁵D. V. Chulhai, Z. Hu, J. E. Moore, X. Chen, and L. Jensen, "Theory of linear and nonlinear surface-enhanced vibrational spectroscopies," Ann. Rev. Phys. Chem. **67**, 541–564 (2016).
- ¹⁶L. Jensen, C. M. Aikens, and G. C. Schatz, "Electronic structure methods for studying surface-enhanced raman scattering," Chem. Soc. Rev. **37**, 1061–1073 (2008).
- ¹⁷A. Campion and P. Kambhampati, "Surface-enhanced raman scattering," Chem. Soc. Rev. **27**, 241–250 (1998).
- ¹⁸S. M. Morton, D. W. Silverstein, and L. Jensen, "Theoretical studies of plasmonics using electronic structure methods," Chem. Rev. **111**, 3962–3994 (2011).
- ¹⁹L. Zhao, L. Jensen, and G. C. Schatz, "Pyridine-Ag₂₀ cluster: A model system for studying surface-enhanced raman scattering," J. Am. Chem. Soc. **128**, 2911–2919 (2006).
- ²⁰S. M. Morton and L. Jensen, "Understanding the molecule-surface chemical coupling in SERS,"
 J. Am. Chem. Soc. 131, 4090–4098 (2009).
- ²¹J. E. Moore, S. M. Morton, and L. Jensen, "Importance of correctly describing charge-transfer excitations for understanding the chemical effect in sers," J. Phys. Chem. Lett. **3**, 2470–2475 (2012).

- ²²N. Valley, N. Greeneltch, R. P. Van Duyne, and G. C. Schatz, "A look at the origin and magnitude of the chemical contribution to the enhancement mechanism of surface-enhanced raman spectroscopy (SERS): Theory and experiment," J. Phys. Chem. Lett. **4**, 2599–2604 (2013).
- ²³R. L. M. Gieseking, J. Lee, N. Tallarida, V. A. Apkarian, and G. C. Schatz, "Bias-dependent chemical enhancement and nonclassical stark effect in tip-enhanced raman spectromicroscopy of co-terminated ag tips," J. Phys. Chem. Lett. **9**, 3074–3080 (2018).
- ²⁴R. L. Gieseking, M. A. Ratner, and G. C. Schatz, "Semiempirical modeling of electrochemical charge transfer," Faraday Discuss. **199**, 547–563 (2017).
- ²⁵R. L. Gieseking, M. A. Ratner, and G. C. Schatz, "Theoretical modeling of voltage effects and the chemical mechanism in surface-enhanced raman scattering," Faraday Discuss. **205**, 149–171 (2017).
- ²⁶A. T. Zayak, Y. S. Hu, H. Choo, J. Bokor, S. Cabrini, P. J. Schuck, and J. B. Neaton, "Chemical raman enhancement of organic adsorbates on metal surfaces," Phys. Rev. Lett. **106**, 083003 (2011).
- ²⁷A. K. Kuhlman and A. T. Zayak, "Revealing interaction of organic adsorbates with semiconductor surfaces using chemically enhanced raman," J. Phys. Chem. Lett. **5**, 964–968 (2014).
- ²⁸A. T. Zayak, H. Choo, Y. S. Hu, D. J. Gargas, S. Cabrini, J. Bokor, P. J. Schuck, and J. B. Neaton, "Harnessing chemical raman enhancement for understanding organic adsorbate binding on metal surfaces," J. Phys. Chem. Lett. **3**, 1357–1362 (2012).
- ²⁹F. W. Hilty, A. K. Kuhlman, F. Pauly, and A. T. Zayak, "Raman scattering from a molecule-semiconductor interface tuned by an electric field: Density functional theory approach," J. Phys. Chem. C **119**, 23113–23118 (2015).
- ³⁰J. R. Lombardi, "The theory of surface-enhanced raman scattering on semiconductor nanoparticles; toward the optimization of sers sensors," Faraday Discuss. **205**, 105–120 (2017).
- ³¹D. Rappoport, S. Shim, and A. Aspuru-Guzik, "Simplified sum-over-states approach for predicting resonance raman spectra. application to nucleic acid bases," J. Phys. Chem. Lett. **2**, 1254, 1260 (2011).
- ³²J. Guthmuller, "Comparison of simplified sum-over-state expressions to calculate resonance raman intensities including franck-condon and herzberg-teller effects," J. Chem. Phys. **144**, 064106 (2016).
- ³³S. Liu, X. Zhao, Y. Li, X. Zhao, and M. Chen, "Density functional theory study on herzberg-teller contribution in raman scattering from 4-aminothiophenol-metal complex and metal-4-

- aminothiophenol-metal junction," J. Chem. Phys. 130, 234509 (2009).
- ³⁴J. B. Cabalo, S. K. Saikin, E. D. Emmons, D. Rappoport, and A. Aspuru-Guzik, "State-by-state investigation of destructive interference in resonance raman spectra of neutral tyrosine and the tyrosinate anion with the simplified sum-over-states approach," J. Phys. Chem. A 118, 9675–9686 (2014).
- J. R. Lombardi and R. L. Birke, "A unified approach to surface-enhanced Raman spectroscopy,"
 J. Phys. Chem. C 112, 5605–5617 (2008).
- ³⁶J. R. Lombardi and R. L. Birke, "A unified view of surface-enhanced raman scattering," Acc. Chem. Res. **42**, 734–742 (2009).
- ³⁷R. Chen and L. Jensen, "Interpreting the chemical mechanism in sers using a raman bond model," J. Chem. Phys. **152**, 024126 (2020).
- ³⁸R. Chen and L. Jensen, "Quantifying the enhancement mechanisms of surface-enhanced raman scattering using a raman bond model," The Journal of Chemical Physics **153**, 224704 (2020).
- ³⁹F. L. Hirshfeld, "Bonded-atom fragments for describing molecular charge densities," Theor. Chim. Acta **44**, 129–138 (1977).
- ⁴⁰G. K. Laura Gagliardi, Roland Lindh, "Local properties of quantum chemical systems: The loprop approach," J. Chem. Phys. **121**, 4494–4500 (2004).
- ⁴¹B. Cordero, V. Gómez, A. E. Platero-Prats, M. Revés, J. Echeverría, E. Cremades, F. Barragán, and S. Alvarez, "Covalent radii revisited," Dalton Trans., 2832–2838 (2008).
- ⁴²P. Philipsen, G. te Velde, E. Baerends, J. Berger, P. de Boeij, M. Franchini, J. Groeneveld, E. Kadantsev, R. Klooster, F. Kootstra, M. Pols, P. Romaniello, M. Raupach, D. Skachkov, J. Snijders, C. Verzijl, J. C. Gil, J. M. Thijssen, G. Wiesenekker, C. A. Peeples, G. Schreckenbach, and T. Ziegler., "Band 2022.1, scm, theoretical chemistry, vrije universiteit, amsterdam, the netherlands, http://www.scm.com," (2022).
- ⁴³G. te Velde and E. J. Baerends, "Precise density-functional method for periodic structures," Phys. Rev. B **44**, 7888–7903 (1991).
- ⁴⁴E. Baerends, T. Ziegler, A. Atkins, J. Autschbach, O. Baseggio, D. Bashford, A. Bérces, F. Bickelhaupt, C. Bo, P. Boerrigter, C. Cappelli, L. Cavallo, C. Daul, D. Chong, D. Chulhai, L. Deng, R. Dickson, J. Dieterich, F. Egidi, D. Ellis, M. van Faassen, L. Fan, T. Fischer, A. Förster, C. F. Guerra, M. Franchini, A. Ghysels, A. Giammona, S. van Gisbergen, A. Goez, A. Götz, J. Groeneveld, O. Gritsenko, M. Grüning, S. Gusarov, F. Harris, P. van den Hoek, Z. Hu, C. Jacob, H. Jacobsen, L. Jensen, L. Joubert, J. Kaminski, G. van Kessel, C. Knig, F. Kootstra, A. Kovalenko,

- M. Krykunov, P. Lafiosca, E. van Lenthe, D. McCormack, M. Medves, A. Michalak, M. Mitoraj, S. Morton, J. Neugebauer, V. Nicu, L. Noodleman, V. Osinga, S. Patchkovskii, M. Pavanello, C. Peeples, P. Philipsen, D. Post, C. Pye, H. Ramanantoanina, P. Ramos, W. Ravenek, M. Reimann, J. Rodríguez, P. Ros, R. Rüger, P. Schipper, D. Schlüns, H. van Schoot, G. Schreckenbach, J. Seldenthuis, M. Seth, J. Snijders, M. Solà, M. Stener, M. Swart, D. Swerhone, V. Tognetti, G. te Velde, P. Vernooijs, L. Versluis, L. Visscher, O. Visser, F. Wang, T. Wesolowski, E. van Wezenbeek, G. Wiesenekker, S. Wolff, T. Woo, and A. Yakovlev, "Adf 2022.1, scm, theoretical chemistry, vrije universiteit, amsterdam, the netherlands, http://www.scm.com." (2022).
- ⁴⁵G. te Velde, F. M. Bickelhaupt, E. J. Baerends, C. Fonseca Guerra, S. J. A. van Gisbergen, J. G. Snijders, and T. Ziegler, "Chemistry with adf," J. Comput. Chem. **22**, 931–967 (2001).
- ⁴⁶A. D. Becke, "Density-functional exchange-energy approximation with correct asymtotic-behavior," Phys. Rev. A **38**, 3098–3100 (1988).
- ⁴⁷J. P. Perdew, "Density-functional approximation for the correlation energy of the inhomogeneous electron gas," Phys. Rev. B **33**, 8822–8824 (1986).
- ⁴⁸E. van Lenthe, E. J. Baerends, and J. G. Snijders, "Relativistic regular two-component hamiltonians," J. Chem. Phys. **99**, 4597–4610 (1993).
- ⁴⁹"The pymol molecular graphics system, version 1.2r3pre, schrödinger, llc." (2019).
- ⁵⁰A. Otto, J. Timper, J. Billmann, and I. Pockrand, "Enhanced inelastic light scattering from metal electrodes caused by adatoms," Phys. Rev. Lett. **45**, 46–49 (1980).
- ⁵¹A. Otto, "The 'chemical' (electronic) contribution to surface-enhanced raman scattering," J. Raman Spectrosc. **36**, 497–509 (2005).